

Is the Redox State of the c_i Heme of the Cytochrome b_6f Complex Dependent on the Occupation and Structure of the Q_i Site and Vice Versa?

Received for publication, March 20, 2009, and in revised form, May 4, 2009. Published, JBC Papers in Press, May 28, 2009, DOI 10.1074/jbc.M109.016709

Agnès de Lacroix de Lavalette^{†1}, Lise Barucq^{†1}, Jean Alric[§], Fabrice Rappaport^{§2}, and Francesca Zito^{‡3}

From the Institut Biologie Physico-Chimique, [†]UMR7099, CNRS/Université Paris-7 and [§]UMR7141, CNRS/Université Paris-6, 13 rue Curie, F-75005 Paris, France

Oxidoreductases of the cytochrome bc_1/b_6f family transfer electrons from a liposoluble quinol to a soluble acceptor protein and contribute to the formation of a transmembrane electrochemical potential. The crystal structure of cyt b_6f has revealed the presence in the Q_i site of an atypical c -type heme, heme c_i . Surprisingly, the protein does not provide any axial ligand to the iron of this heme, and its surrounding structure suggests it can be accessed by exogenous ligand. In this work we describe a mutagenesis approach aimed at characterizing the c_i heme and its interaction with the Q_i site environment. We engineered a mutant of *Chlamydomonas reinhardtii* in which Phe⁴⁰ from subunit IV was substituted by a tyrosine. This results in a dramatic slowing down of the reoxidation of the b hemes under single flash excitation, suggesting hindered accessibility of the heme to its quinone substrate. This modified accessibility likely originates from the ligation of the heme iron by the phenol(ate) side chain introduced by the mutation. Indeed, it also results in a marked downshift of the c_i heme midpoint potential (from +100 mV to –200 mV at pH 7). Yet the overall turnover rate of the mutant cytochrome b_6f complex under continuous illumination was found similar to the wild type one, both *in vitro* and *in vivo*. We propose that, in the mutant, a change in the ligation state of the heme upon its reduction could act as a redox switch that would control the accessibility of the substrate to the heme and trigger the catalysis.

The cytochrome b_6f complex of oxygenic photosynthesis is the integral membrane protein, the quinol:plastoquinone oxidoreductase activity of which allows the linear electron flow between the two photosystems (PSI and PSII).⁴ The turnover of the cytochrome b_6f complex depends on the steady state of its redox partners, the liposoluble plastoquinol (PQH₂ reduced and protonated plastoquinone PQ) formed by the PSII, and the hydrosoluble plastoquinone oxidized by the PSI. In the Q_o site, exposed to the luminal side, the quinol is oxidized, and this oxidation is coupled to the release of two protons into the

lumen. The two electrons provided by the quinol are transferred along two bifurcated pathways, the high and low potential chains. The high potential chain involves two luminal redox partners, the membrane-anchored flexible Rieske [2Fe-2S] cluster and the cytochrome f , which ultimately interacts with the soluble plastocyanin. In the low potential chain, electrons are transferred to the stroma via the low and high potential b hemes (b_L and b_H) of the transmembrane b_6 subunit. Two turnovers of the cyt b_6f complex lead to the reduction of the low potential chain, thereby allowing the reduction of a quinone molecule in the stromal Q_i pocket. This mechanism, which recycles reducing equivalents, is referred to as the “Q cycle,” initially described by Mitchell (1) and modified later by Crofts *et al.* and others (2, 3).

Although this quinol:cytochrome oxidoreductase activity is involved in both the respiratory and photosynthetic electron transfer chains, recent x-ray data (4–6) have evidenced major structural differences between the b_6f complex and its mitochondrial counterpart the bc_1 complex (for reviews see Refs. 7–10). Indeed an additional heme localized in close contact with heme b_H stands as another putative electron carrier as proposed earlier by Lavergne (11). Since it was brought to light by the x-ray studies, knowledge of the basic properties of this heme, named c_i in reference to the Q_i site (5) or c_n in reference to its proximity to the negatively charged side of the membrane (4), has significantly improved. The proteins involved in the assembly machinery of the heme have been identified in *Chlamydomonas reinhardtii* and *Arabidopsis thaliana* (12, 13). Consistent with the structure, according to which the only axial ligand could be a water molecule interacting with the propionate chain of the b_H heme, the spectroscopic properties of this heme are those of a high spin heme (14, 15). Evidences for a high spin heme covalently bound to the cytochrome b subunit were also found in *Heliobacterium modesticaldum* and *Heliobacillus mobilis* (16).

In the b_6f complex from the oxygenic photosynthetic chain, EPR (15) and structural data (17) have shown that NQNO (2-*n*-nonyl-1-4-hydroxyquinoline *N*-oxide), an inhibitor of the Q_i pocket (18, 19), can act as an axial ligand to c_i . This ligation is accompanied by a significant change in the redox properties of c_i , because, in the presence of NQNO, at least two titrations waves were observed (13, 14), one with a midpoint potential (E_m) similar to that observed in the absence of NQNO and the other with a midpoint potential downshifted by ~250 mV. This, together with the widespread range of redox potential

¹ Both authors contributed equally to this work.

² To whom correspondence may be addressed. E-mail: Fabrice.Rappaport@ibpc.fr.

³ To whom correspondence may be addressed. E-mail: Francesca.Zito@ibpc.fr.

⁴ The abbreviations used are: PSI, photosystem I; PSII, photosystem II; b_H , high potential heme b ; b_L , low potential heme b ; NQNO, 2-*n*-nonyl-4-hydroxyquinoline *N*-oxide; PQ, plastoquinone; cyt, cytochrome; Tricine, *N*-(2-hydroxy-1,1-bis(hydroxymethyl)ethyl)glycine; WT, wild type.

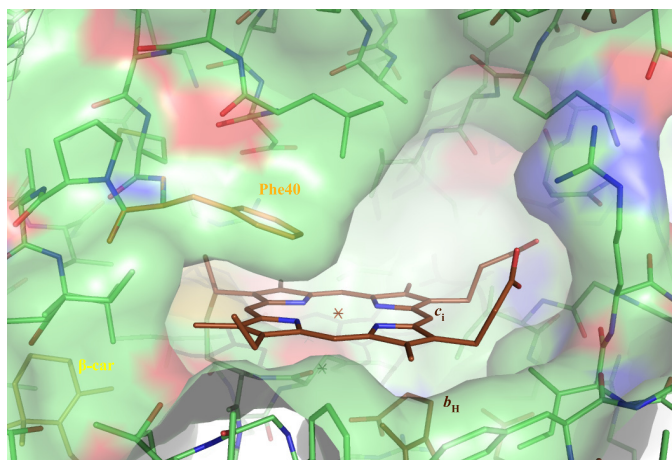


FIGURE 1. A view of the Q_i site from the dimer interface. The coordinates are from the Protein Data Bank 1Q90 model. The Van der Waal's surface of the peptide chains was drawn with Pymol. Phe⁴⁰ is in van der Waal's contact with the plane of the c_i heme.

found for heme c_i (11, 14, 15, 20), points to a structural plasticity of the c_i ligand network.

This plasticity may arise from the unusual coordination properties of the heme c_i. As a matter of fact, the x-ray models of the complex from *C. reinhardtii* and *Mastigocladus laminosus* evidenced a water or hydroxyl molecule as a fifth ligand. The sixth position of coordination is directed toward the Q_i pocket and appears as free. Nevertheless, the side chain of Phe⁴⁰ of subunit IV protrudes above the heme plane, leaving little space for any axial ligand to the heme c_i. Besides, modeling a quinone analogue in the electron density found in the Q_i pocket of structures obtained in presence of Tridecyl- Stigmatellin or NQNO implies a steric clash with the native position of the Phe⁴⁰ aromatic ring.⁵ The Phe⁴⁰ residue of subunit IV therefore stands as a key residue for the plasticity of the site, making it an ideal mutagenesis target when attempting to alter the possible interactions between c_i and the quinone or quinol (4, 5) (Fig. 1). Here we present the consequences of the substitution of Phe⁴⁰ by a tyrosine on the properties and function of the c_i heme.

EXPERIMENTAL PROCEDURES

Strains, Media, and Growth Conditions—The H₆F₅ strain (mt⁺), expressing a cytochrome *f* version histidine tagged at its C-terminal end (21), and the Δ*petD* (mt⁺) deletion strain (22) were used as recipient strains in chloroplast transformation experiments. H₆F₅, Δ*petD*, and mutant strains were grown on Tris-acetate-phosphate medium (pH 7.2) at 25 °C under dim light (5–6 μE·m⁻²·s⁻¹) (23). The H₆F₅ strain was used as a wild type reference in all experiments.

Plasmids, Oligonucleotides, and Mutagenesis—The pWQH₆ plasmid, carrying the entire *petD* sequence, together with the C-terminal end of the sequence coding for histidine-tagged cytochrome *f* was obtained by ligation of the 0.55-kb EcoRV-AccI fragment recovered from plasmid pFWH₆ (5) into the corresponding sites of plasmid pdWQ (21).

The mutated version of the *petD* gene was created by PCR-mediated site-directed mutagenesis. Plasmid pdΔHI.I (22), car-

rying the entire *petD* coding sequence was used as a template in PCRs performed with ArrowTM *Taq* DNA polymerase, employed according to the manufacturer's instructions, using the primers: DirF40Y (5'-GGGTGGCCAAACGATTTAT-TATACATGTACCCTGTTGTTATTTTAGGTACATTT-3') and RevQ_i (5'-GGGTGGCCAAAGCAGGTTTAC CGTAAAGT-GTT-3'), where nucleotides written in bold differ from the WT sequence. The PCR product was digested with MscI (a single restriction site underlined in the sequence of the primers) and religated onto itself to yield plasmid pdΔHF40Y. This plasmid was digested with HindIII and NcoI, and the resulting 833-bp fragment was ligated into the corresponding sites of plasmid pWQH₆ to yield plasmid pdF40Y. Plasmid pdK-F40Y was constructed by introducing the 1.9-kb SmaI-EcoRV *aadA* cassette (24), in the same orientation as the *petD* gene, into the EcoRV site of plasmid pdF40Y.

Chloroplast Transformation in *C. reinhardtii*—The Δ*petD* (22) and H₆F₅ (21) strains were transformed by tungsten particle bombardment according to Boynton *et al.* (25). When using plasmid pdF40Y to bombard the non-photosynthetic Δ*petD* strain, transformed clones were selected on minimum medium at 60 μE·m⁻²·s⁻¹. When using plasmid pdK-F40Y to bombard the H₆F₅ strain, transformants were selected on Tris-acetate-phosphate medium supplemented with spectinomycin (100 μg·ml⁻¹). Transformed cells were subcloned several times on selective medium until they reach homoplasmy, assessed by restriction fragment length polymorphism analysis of specific PCR fragments (26).

Preparative and Analytical Techniques—Cells grown to a density of 4 × 10⁶ ml⁻¹ were broken in "bead beater" (Biospec-Products) according to the manufacturer's instructions. The membrane fraction was collected by centrifugation and resuspended in 10 mM Tricine, pH 8, at a chlorophyll concentration of 3 mg·ml⁻¹. For SDS-PAGE, the membrane proteins were resuspended in 100 mM dithiothreitol and 100 mM Na₂CO₃ and solubilized by 2% SDS at 100 °C for 1 min. Polypeptides were separated on a 12–18% polyacrylamide gel containing 8 M urea. Immunoblotting was performed as described in Pierre *et al.* (27).

Cytochrome *b*₆*f* complexes were isolated as described in Ref. 5 and titrated accordingly to Alric *et al.* (14). *In vitro* electron transfer activity was measured as described in Ref. 27. Cytochrome *b*₆*f* complexes were analyzed by size exclusion chromatography in 20 mM Tris-HCl, pH 8.0, 250 mM NaCl, 0.2 mM C12M onto an exclusion Superdex 200 HR Amersham Biosciences column (28).

Fluorescence Induction Measurements—The phenotype of *b*₆*f* mutants was characterized by their fluorescence induction kinetics. The measurements were performed at room temperature on a home-built fluorimeter, with continuous illumination at 520 nm and fluorescence detection in the far-red region (29–31).

Spectroscopy—Time-resolved light-induced absorbance changes in whole cells of *C. reinhardtii* were monitored with a pulsed differential LED spectrophotometer JTS 10 Bio-Logic, whereas redox-induced and CO-induced absorbance changes in purified *b*₆*f* preparations were measured with a xenon flash lamp spectrophotometer, as previously described respectively

⁵ D. Picot, personal communication.

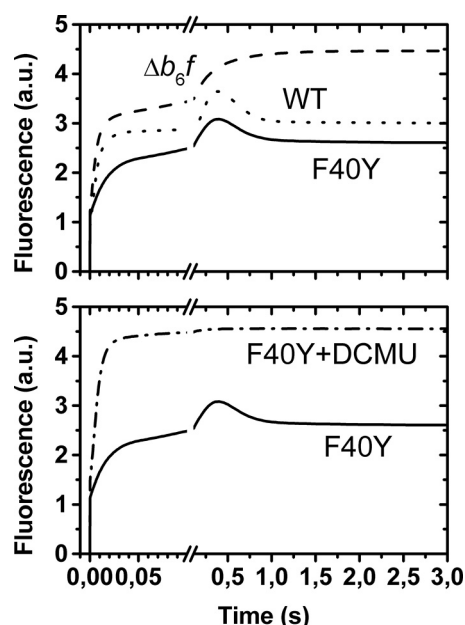


FIGURE 2. Fluorescence induction curves under aerobic conditions. The top panel displays the light-induced fluorescence changes in the WT (dotted curve), in a mutant lacking the *b₆f* complex (dashed curve), and in the F40Y mutant (solid curve). In the latter, at variance with the *b₆f* lacking mutant, the light-induced fluorescence does not reach the F_{max} level, as illustrated in the bottom panel, which displays the fluorescence changes observed in the F40Y mutant in the absence (solid curve) and presence (dashed-dotted curve) of 3-(3,4-dichlorophenyl)-1,1-dimethylurea (DCMU, 10 μ M).

by Joliot *et al.* (32) and in Alric *et al.* (14). To characterize the kinetics of CO binding after laser flash photolysis, the purified *b₆f* complex (5 μ M, pH 8) was thoroughly degassed, then reduced by addition of dithionite, and then equilibrated with \sim 1 atm of CO.

Cytochrome *b* redox changes were measured in the presence of NQNO to obtain full inhibition of cytochrome *b₆* oxidation. NQNO was synthesized in the laboratory according to the procedure described in Ref. 33. FOS-choline-14 (*n*-tetradecylphosphocholine) was purchased from Anatrace.

RESULTS

Construction of *C. reinhardtii* Mutants Expressing a Mutated *petD* Gene—We investigated by site-directed mutagenesis the importance of the accessibility to the heme *c_i* by replacing the Phe⁴⁰ of subunit IV, in van der Waal's contact with the plane of the *c_i* heme, by a tyrosine. Our first attempt to recover phototrophic clones following transformation of the Δ *petD* strain with plasmid pdF40Y proved unsuccessful. As an alternative strategy, we used the histidine-tagged *H₆F₅* strain as a recipient strain for transformation with the pd-KF40Y plasmid and recovered transformed clones on spectinomycin supplemented medium (24). Five independent dK-F40Y clones, hereafter referred to as F40Y mutants, were brought to homoplasmy with respect to the *petD* mutation. Because transformation of the Δ *petD* strain by the mutated copy of the *petD* gene failed to rescue phototrophic growth, we expected the recovered homoplasmic transformants to display fluorescence induction kinetics typical of mutants lacking cytochrome *b₆f* activity (30, 31, 34). Surprisingly, they still displayed unimpaired fluorescence induction kinetics (Fig. 2) (26). They grew as the wild type

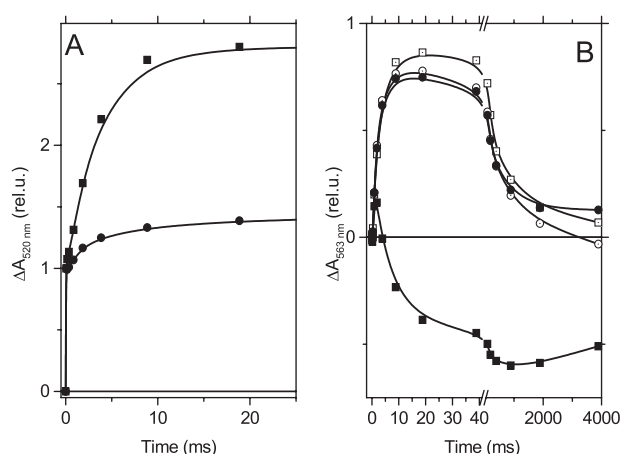


FIGURE 3. Flash-induced kinetics of electron transfer in the low potential chain of WT and F40Y *cyt b₆f* complexes. A, the flash-induced absorption changes at 520 nm, which reflect the transient changes in the transmembrane electric field, in the WT (squares) and in the F40Y mutant (circles). B, the flash-induced absorption changes at 563 nm, which reflects the redox changes of the *b* hemes in the WT (squares) and in the F40Y mutant (circles) in the absence (solid symbols) and presence (open symbols) of NQNO (50 μ M).

on minimum medium and did not show any photo-sensitivity under high light (200 μ E·m⁻²·s⁻¹), neither in photoautotrophic nor in mixotrophic conditions (data not shown). On this basis, we expected the electron transfer chain to be active and assessed its function by time-resolved absorption spectroscopy.

Flash-induced Kinetics—Fig. 3A shows the slow electrogenic phase associated with the turnover of the *b₆f* complex in WT and mutant strains. At 100 μ s the absorption changes result from the charge separation event at the level of PSI; the subsequent electrogenic phase that develops with a \sim 2-ms half-time witnesses the cytochrome *b₆f* turnover (35, 36). In the F40Y mutant, the amplitude of this phase was dramatically decreased.

We then measured the kinetics of the absorption changes associated with the redox changes of the *b* hemes, at 563 nm (Fig. 3B). In the WT, in the absence of inhibitors, a transient reduction (upward signal) is followed by a pronounced oxidation phase (downward signal). The negative signal observed 1 s after a flash shows that the overall reaction results in the net oxidation of a *b* heme. Thus, in these experimental conditions, the *b_H* and *b_L* hemes were respectively reduced and oxidized in the dark, so that the injection of one electron into the low potential chain allowed the reduction of a quinone at the *Q_i* site and the associated oxidation of the two *b* hemes. The addition of NQNO (50 μ M) slows down this latter reaction and, accordingly, allows the observation of the full extent of the *b* heme reduction phase (37). In the mutant, in the absence of NQNO, we observed a pronounced reduction of *b* heme with a half-time of \sim 2 ms similar to the one observed in the WT in the presence of NQNO, followed by a very slow oxidation phase. The addition of NQNO had no further effect on this oxidation phase. This result, together with the decreased amplitude of the electrogenic phase, indicates that in the mutant, under the conditions of the experiments, the *b_H* heme was likely reduced in the dark, whereas the *b_L* heme was oxidized and that quinol oxidation at the *Q_o* site operated normally. The dramatic slow down of the oxidation of the *b* hemes indicates that quinone

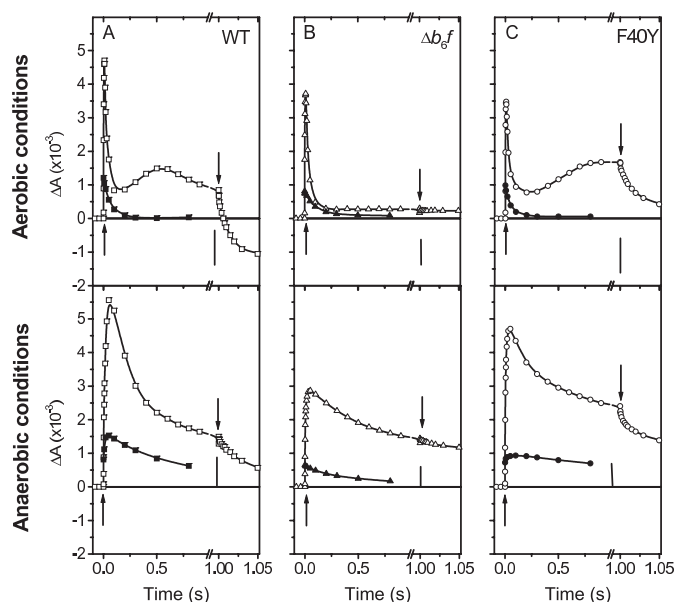


FIGURE 4. Light-induced changes of the transmembrane electric field under continuous illumination. The left, middle, and right panels, respectively show the data obtained with the WT, with a mutant lacking *b₆f* and with the F40Y mutant. The light was switched on and off as indicated by upward and downward arrows, respectively. In each column, the top and bottom panels show the results obtained in aerobic and anaerobic conditions, respectively. Flash-induced kinetics (closed symbols) are also shown under the same conditions to provide a calibration of the light intensity. The amplitude corresponding to one electron transferred by photosystem I (phase *a*) is depicted by a vertical bar.

reduction at the *Q_i* site is strongly affected, consistent with the quasi absence of electrogenic phase. The F40Y mutation thus seems to cause a strong inhibition of the *Q_i* site. Yet contrasting results were obtained when studying the turnover of the *b₆f* complex under continuous illumination.

Continuous Light Measurements—As shown above, the fluorescence induction curves of F40Y cells are virtually indistinguishable from that commonly obtained with WT. Fig. 2 shows typical measurements carried out under aerobic conditions in the presence or absence of 3-(3,4-dichlorophenyl)-1,1-dimethylurea. Surprisingly, in the F40Y mutant, the steady state fluorescence level, reached after a few seconds of illumination, was similar to the WT one. Thus, despite the apparent loss of *Q_i* site activity, as observed under single turnover flash experiments, the electron flows through the cytochrome *b₆f* complex are similar in both strains.

It is of note however that the fluorescence measurements were performed under aerobic conditions (oxidized PQ pool), whereas the flash-induced kinetics were obtained under anaerobic conditions (reduced PQH₂ pool), leaving open the possibility of a different occupancy of the *Q_i* site by its substrate in the two experiments.

We thus measured the overall activity of the photosynthetic chain during illumination under saturating light intensity, in aerobic as well as anaerobic conditions. In such conditions, the limiting step of the photosynthetic electron flow bears on the cytochrome *b₆f* complex. Electrochromic changes of carotenoids, measured at 520 nm, were used as a probe of the transmembrane potential (38). As shown in Fig. 4 the time course of the absorption changes encompasses a very fast rise (with an

initial slope of 1000 charges translocated per second), because of the charge separation at the level of the photosynthetic chain (PSII-PQ-*b₆f*-plastocyanin-PSI), followed by a decay likely reflecting the activation of CF₀-CF₁ ATP synthase. After ~1 s of illumination, the membrane potential reaches a quasi-steady state regime where the generation of the transmembrane electric field by the activity of the photosynthetic chain nearly compensates its dissipation by the ATP synthase. When the light is switched off, the photochemical process is instantaneously stopped, and the absorption changes decay as the transmembrane potential is rapidly consumed by the CF₀-CF₁ ATP synthase. The difference between the slopes of the signal before and after the light is switched off is indicative of the photochemical activity (38, 39). We first validated this approach by the study of a *b₆f* lacking mutant (Fig. 4B). Switching off the illumination did not induce any variation of the slope of the electrochromic band shift after 1 s of illumination. In the WT and in the F40Y mutant (Fig. 4, A and C), under aerobic and anaerobic conditions, a clear change in the slope was observed when the light was switched off, showing that, under illumination, the consumption of the transmembrane potential by the ATP synthase is compensated by its photo-induced formation. In the WT, after normalization of the change in slope by the signal induced by a single turnover flash (which yields the absorption changes resulting from the transfer of 2 electrons across the membrane), we estimated the photochemical activity to ~100 e⁻·s⁻¹ (aerobic) and 40 e⁻·s⁻¹ (anaerobic). In the mutant, these rates were estimated to 70 and 40 charges/s, respectively.

At this stage we are thus confronted to an apparent paradox. On the one hand, the quinone reduction activity of the *Q_i* site is strongly impaired as observed in the flash experiments. On the other hand, the overall activity of the mutated *b₆f* complex only slightly differs from the WT one under continuous illumination, suggesting that the functional constraints underlying the blockage of the *Q_i* site function under single flash conditions are relieved in a continuous illumination regime. To obtain a more complete picture of the interaction between the Tyr side chain and the *c_i* heme, we studied the physico-chemical properties of the *c_i* heme in purified *b₆f* complex from the mutant.

Biochemical Characterization of the F40Y Mutant—The mutant accumulated the major subunits of the cytochrome *b₆f* complex at approximately wild type levels (Fig. 5A). In particular the content in subunit IV, which harbors the mutations, was unaltered. To further identify the *c_i* heme associated with cyt *b₆*, the gels were stained with 3,3',5,5' tetramethylbenzidine, a specific staining for hemes (40). The peroxidase activity associated with cyt *b₆* proved to be SDS-resistant consistent with the covalent binding of a heme to this subunit, strongly supporting the presence of the *c_i* heme. The oligomerization state of the cytochrome *b₆f* complex, as measured by size exclusion chromatography, was not affected by the mutation (Fig. 5B).

The *b₆f* complex purified from the mutant was then tested for its ability to mediate the transfer of electrons between plastoquinol and oxidized plastocyanin *in vitro*. Its activity (~350 e⁻·f⁻¹·s⁻¹) was found similar to that of the wild type complex (~400 e⁻·f⁻¹·s⁻¹). This is satisfyingly consistent with the conclusion drawn from the *in vivo* activity, described above, that

Q_i Site Function in Cytochrome *b₆f* Complex

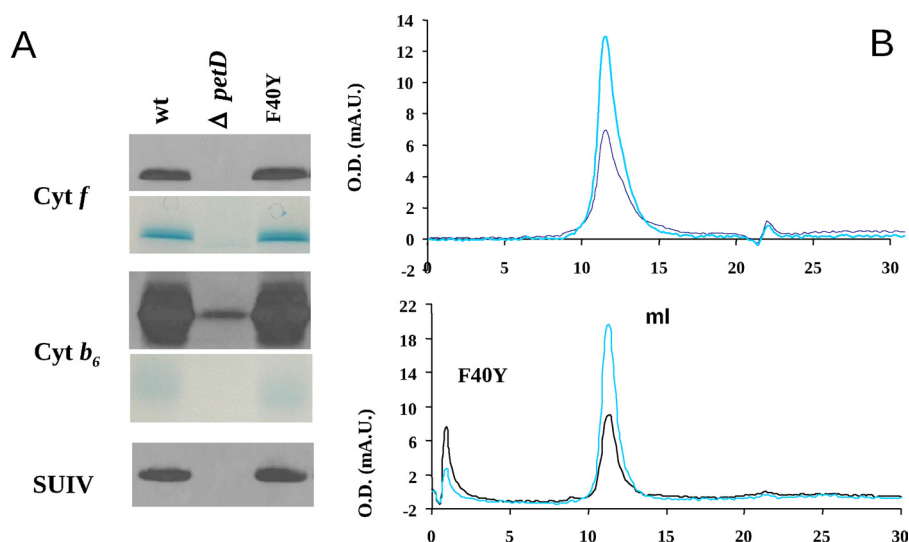


FIGURE 5. **Biochemical characterization of cytochrome *b₆f* complex mutants.** *A*, immunoblot and specific heme staining (for *cyt f* and *cyt b₆*) of membrane protein extracts. The membranes were probed with specific antibodies against cytochrome *f*, cytochrome *b₆*, and subunit IV. Loads for each sample correspond to 20 μ g of chlorophyll. *B*, size exclusion chromatography of WT and dF40Y mutant *b₆f* complex, analyzed on a 10 \times 300-mm Superdex 200 HR column. The absorbance of the eluate was monitored at 280 (black line) and 420 (cyan line) nm.

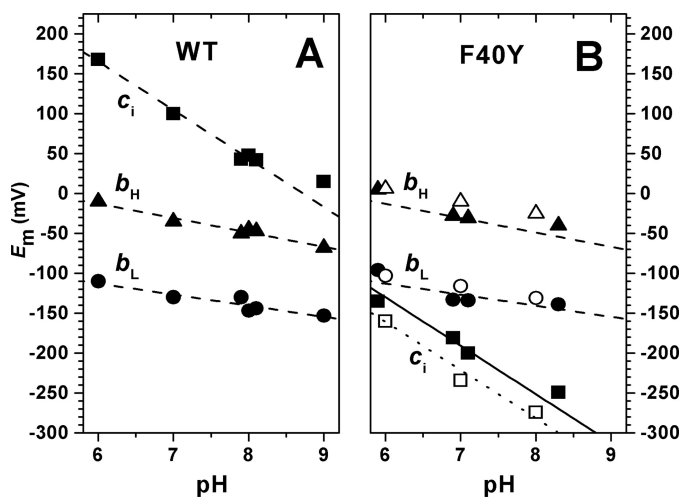


FIGURE 6. **pH dependence of the midpoint potentials of cofactors in the low potential chain of WT (A) and F40Y (B) *cyt b₆f* complexes:** *b_L* (solid circles), *b_H* (solid triangles), and *c_i* (solid squares). The open symbols in B show the midpoint potentials of the three hemes in the presence of NQNO (50 μ M). In both the absence and presence of NQNO the midpoint potential of *c_i* depends upon pH with a slope of 60 mV per pH unit.

the turnover rate of the mutated complex hardly differs from the WT one.

Redox and Spectral Characteristics of Heme *c_i*—The substitution of the Phe⁴⁰ by a Tyr has no effect on the midpoint potentials of the *b_L* and *b_H* hemes but strongly modifies the E_m of heme *c_i* (Fig. 6B), which was downshifted from +100 mV in the WT to –200 mV in the mutant (at pH 7.0). As for the WT (Fig. 6A), the midpoint potential was pH-dependent with a slope of –60 mV/pH unit (Fig. 6B).

The F40Y mutation also affected the (oxidized – reduced) spectrum of the *c_i* heme (Fig. 7A), which displays a shoulder around 440 nm and an overshoot at 380 nm. These features were even more pronounced after the addition of NQNO (Fig. 7B) and likely reflect changes in the heme environment. In addition

to this spectroscopic change, the addition of NQNO also induced a moderate downshift of the midpoint potential of the *c_i* heme in the mutant (Fig. 6B, open squares). However, the amplitude of this downshift was much smaller than that previously reported in the WT, and the corresponding titration curve was satisfyingly fit with a $n = 1$ Nernst curve, whereas in the WT the titration curve was split into at least two waves (14, 15). Yet the strong modifications of the midpoint potential of *c_i* and the spectroscopic changes of its (oxidized – reduced) spectrum point to a significant change in the environment of the heme in the F40Y mutant, which can still accommodate quinones/analogues.

Carbon Monoxide Binding—Carbon monoxide can bind to the

reduced state of most high spin hemes, including *c_i*, as witnessed by the blue shift of its Soret band (14, 19). The reduced F40Y complex was able to bind CO, because incubation in ~100% CO resulted in the appearance of a pronounced shoulder at ~410 nm. To assess the hindrance resulting from the F40Y mutation more directly, we measured the kinetics of CO rebinding after its photodissociation by a laser flash (Fig. 8). As regards to the WT, we note that the kinetics of CO rebinding presented here are significantly slower than those previously reported in (14). This likely reflects changes in the structural integrity of the *b₆f* complex in the previously reported experiments, because we could mimic (not shown) similarly fast rebinding kinetics after the addition of FOS-choline 14, a detergent known to induce the progressive dissociation of the complex.⁶ As shown in Fig. 8, the rebinding of CO was only 2-fold slower in the F40Y mutant than in the WT.

DISCUSSION

Structural Modification of the Near Environment of *c_i* in the F40Y Mutant—We designed the F40Y mutant with the aim to provide a proteic axial ligand to the heme *c_i*. Data from the redox titration suggest that this goal was achieved. Indeed, a coordination link between the phenol(ate) side chain and the heme iron would account for the strong downshift in midpoint potential of heme *c_i*; the phenol(ate) side chain, a strong electron donor group should stabilize the ferric form of the heme and thus lower its midpoint potential, as observed in tyrosine mutants of heme oxygenase and myoglobin (41, 42). Moreover, previous reports showed that NQNO could act as an axial ligand to the WT heme *c_i* (15) and that this inhibitor induces a strong downshift in redox potential (14). In this respect, the consequences of the F40Y mutation are similar to the addition of NQNO. However, whereas upon the addition of NQNO, the

⁶ Y. Pierre, personal communication.

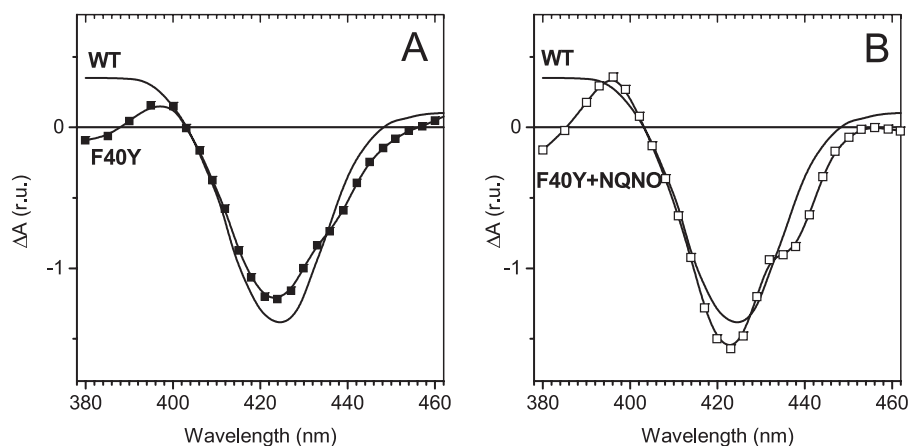


FIGURE 7. Spectral characteristics of the *c₁* heme in WT (solid curve) and F40Y (squares) *cyt b₆f* complexes. A, (oxidized – reduced) spectra of the *c₁* heme obtained as the difference between the absorption spectra measured at 240 and 90 mV for the WT *b₆f* complex (at pH 7.0) and –250 and –400 mV for the F40Y *b₆f* complexes (at pH 9.0). B shows the corresponding spectra for WT and F40Y *b₆f* complexes in the presence of NQNO (50 μ M).

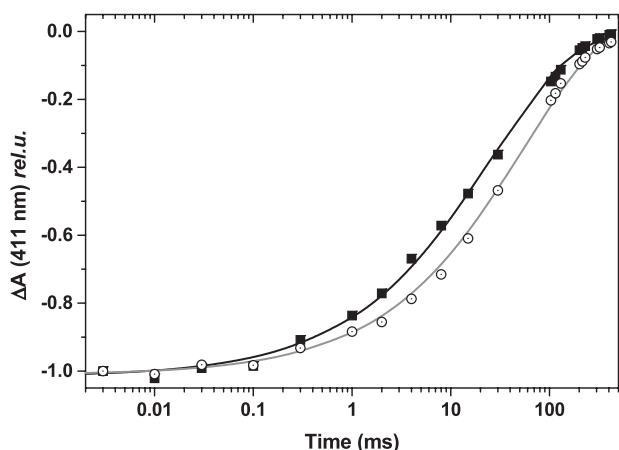


FIGURE 8. Kinetics of CO recombination after photolysis, followed at 411 nm, for the WT (solid squares) and the F40Y mutant (open circles). The kinetics were normalized to their initial amplitude. For qualitative comparison purposes we fitted the data with a stretched exponential ($\exp(-t/\tau^n)$) (gray lines), and this fit yielded: for the WT, $\tau = 25$ ms and $n = 0.5$; for the F40Y, $\tau = 52$ ms and $n = 0.6$.

titration curve was split into two $n = 1$ waves, the redox titration of *c₁* in the mutant was satisfyingly fitted by a single $n = 1$ Nernst curve, both in the presence and absence of NQNO. On a redox standpoint, the ligation state of *c₁* would thus be more homogenous in the mutant than in the WT in the presence of NQNO. The pronounced shoulder at ~ 440 nm, which is enhanced upon addition of NQNO in the (reduced – oxidized) spectrum of *c₁* (Fig. 7), could, however, be taken as an indication of static disorder in the near environment of the heme. Yet a split Soret band of high spin *c* type cytochrome has been previously assigned to a non-degenerate Soret electronic transition, resulting from electronic inequivalency in the *x* and *y* directions of the heme (43, 44), without implying any heterogeneity of the sample. Irrespective of the precise origin of these spectroscopic modifications, the addition of NQNO slightly modifies the spectroscopic as well as the redox properties of *c₁*, showing that the *Q_i* site can accommodate this (semi)quinone analogue, which can interact with *c₁*.

The Functional Consequences of the F40Y Mutation—According to the above proposal that the tyrosine side chain likely acts as a ligand to the *c₁* heme, the accessibility to the heme is expected to be significantly hindered, and this should have significant functional consequences. We found that the reoxidation of the *b* hemes was dramatically slowed down when Phe⁴⁰ was substituted by Tyr (Fig. 3B). The decreased amplitude of the slow electrochromic phase (Fig. 3A) shows that, under our experimental conditions, *b_H* is reduced in the dark so that the cytochrome *b* reduction phase can be ascribed to the reduction of the *b_L* heme. Yet although

the low potential chain was normally fed in reducing equivalents in the mutant, as shown by the WT-like reduction rate of the *b* hemes, the reoxidation of the *b* hemes occurred in the hundreds of ms time range, *i.e.* more than 50-fold more slowly than in the WT. This is consistent with the above hypothesis according to which the *c₁* heme is ligated by the Tyr side chain in the mutant and thereby prevents the access of the quinone to its reduction site. Further, it shows that, provided a quinone is present in the site, the direct electron transfer from *b_H* to the quinone cannot occur with a reasonable rate. At first sight, these proposals are contradicted by the puzzling finding that under continuous illumination the overall activity of the *b₆f* complex is far less decreased (Fig. 4). Interestingly, inhibiting the wild type *Q_i* site with NQNO efficiently slows down the reoxidation of the *b* hemes after a single turnover flash but does not prevent the linear electron flow under steady state illumination (45).

As a possible way to reconcile these apparently contradicting findings, one could consider that the *Q_o* site carries out its role in the quinol-plastocyanin oxidase pathway even though the *Q_i* site is blocked. Such a hypothesis could be in line with the fact that the *bc₁* complex can also sustain electron transfer between quinol and oxidized cytochrome *c* when the *Q_i* site is blocked by antimycin (46). However, the rate sustained in the presence of antimycin is only 2% of that obtained in its absence (47, 48). Given the large structural homology between the *bc₁* and *b₆f* complex regarding the *Q_o* site (which should be qualified however by the different sensitivities to inhibitors such as myxothiazol), blocking the *Q_i* site in the *b₆f* complex should as severely impair the steady state rate of the *Q_o* site turnover, yielding overall turnover rates far lower than those observed here under continuous illumination.

More plausibly, the structural hindrance that accounts for the slowing down of this rate under flash experiments may be, at least partially, relieved under steady state conditions. In other terms, the quinone reduction might be triggered by the illumination regime. What could be the molecular bases of such a switch? As discussed above, the strong downshift of the midpoint potential of *c₁* resulting from the Tyr for Phe substitution

Q_i Site Function in Cytochrome *b₆f* Complex

implies that the Tyr side chain provides stabilization energy to the oxidized state of the heme. On thermodynamic grounds, this means that the interaction between the heme and the phenol(ate) side chain is weakened upon reduction of the heme. This change in the ligation bond strength upon reduction of c_i would readily account for our observations. Indeed, considering the respective midpoint potential of the three hemes in the low potential chain, the F40Y mutation should favor the oxidized state of c_i even under anaerobic conditions (when b_H is reduced but b_L oxidized). Being ligated by the phenol(ate) the midpoint potential of c_i is more negative than that of b_L ; the injection of one electron into the low potential chain results in the reduction of b_L and hardly affects either the redox state of c_i or its ligation state. Thus, the accessibility of the c_i heme to a quinone is hindered, and quinone reduction cannot take place with a reasonable rate. Under continuous illumination, however, the cytochrome *b₆f* complex is submitted to a stronger reducing pressure, which may eventually lead to the reduction of c_i , thereby decreasing the ligation strength. This will allow a quinone to displace the Tyr side chain, access the c_i heme, and then be reduced. Moreover, assuming that the redox potential of the non-ligated c_i is indeed more positive than that of the ligated heme, the reducing pressure continuously undergone by the *b₆f* mutant complex under illumination should significantly increase the steady state concentration of the reduced and weakly ligated heme with respect to the dark-adapted case. Reduction of c_i thus weakens the gate for quinone reduction at the Q_i site, and the electron flux that ensues would keep the reducing pressure high enough to maintain the gate open.

The binding kinetics of CO to the reduced c_i supports this model. Indeed, the moderate decrease of the CO binding rate in the mutant with respect to the WT (2-fold) suggests that the Tyr side chain only weakly hinders the accessibility of CO to the reduced iron. The possibility that the CO replaces the water molecule on the other face of the heme appears less likely because of steric constraints.

In myoglobin or in the cd_1 nitrite reductase from *Pseudomonas aeruginosa*, mutating the distal histidine resulted in a 7–10-fold increase of the CO rebinding rate (49, 50). The magnitude of these kinetic changes provides a reasonable estimate for the sensitivity of the CO binding rate to moderate modifications of the accessibility to the heme. In the cd_1 nitrite reductase from *P. aeruginosa* the targeted His does not directly interact with the heme iron but rather provides steric hindrance (50). In hemoglobin, the distal His also controls the access to the heme via a weak H-bond (51). Thus, if the Tyr⁴⁰ remained a strong axial ligand to the reduced c_i in the mutant *b₆f* complex, it would likely result in a pronounced decrease of the CO rebinding rate. The finding that this is not the case strongly backs up the proposal that, when reduced, c_i is not or weakly ligated by the Tyr side chain and that it can be more easily displaced than when oxidized.

Weakening the ligation strength upon reduction to the ferrous state has already been documented; in mutated heme oxygenase or myoglobin, where the natural His heme ligand was substituted for a Tyr (41, 52), it has been shown that the tyrosinate ligand dissociates upon reduction. Moreover, in the case of the d_1 heme of the cd_1 nitrite reductase (53), the change in the

ligation state undergone by the heme upon its reduction to the ferrous state was proposed to act as a redox switch that controls the accessibility of the substrate to the heme and triggers the catalysis.

Conclusion—We propose that a redox switch is at work to allow the quinone reductase activity in the F40Y mutant. Likewise, the hypothesis that the interaction between the (semi)quinone and c_i is controlled by the redox state of the heme in the WT *b₆f* complex is attractive.

In the WT *b₆f* complex, modeling a quinone in the Q_i site results in a steric clash with the native position of the Phe⁴⁰ aromatic ring,⁵ which has to move to provide access to the sixth ligand position. As a consequence, energy must be provided to allow the interaction between c_i and the (semi)quinone. In analogy with the mechanism proposed here, according to which the ligation state of c_i is linked to its redox state, this “interaction energy” could be provided by the redox state of the heme.

In addition, such a redox-dependent interaction between the quinone and c_i would make the midpoint potentials of both c_i and the quinone/semiquinone dependent on their interaction. If the quinone interacts more strongly with the c_i heme in its oxidized state than in its reduced one, then the oxidized c_i should stabilize the quinone, making the semiquinone more difficult to form. In brief, a stronger reducing redox potential would be required to inject an electron in the interacting quinone- c_i ensemble than in the quinone or c_i heme alone. In addition, the injection of a single electron in this ensemble would weaken the interaction between the two partners, raising their midpoint potential and facilitating the injection of a second electron. Extrapolating to the WT the present evidence that, in the mutant, the ligation state of c_i depends on its redox state and vice versa thus provides a mechanistic insight into the proposal that c_i would force the quasi-concerted reduction of the quinone into a quinol at the expense of the two *b* hemes (15, 54).

Acknowledgments—We are grateful to Frauke Baymann, Yves Choquet, and Daniel Picot for critical reading of the manuscript and fruitful discussions. Thanks are also due to F. Giusti for kindly providing the NQNO and to C. Lebreton for help with biochemical preparations.

REFERENCES

1. Mitchell, P. (1975) *FEBS Lett.* **56**, 1–6
2. Crofts, A. R., and Meinhardt, S. W. (1982) *Biochem. Soc. Trans.* **10**, 201–203
3. Osyczka, A., Moser, C. C., and Dutton, P. L. (2005) *Trends Biochem. Sci.* **30**, 176–182
4. Kurisu, G., Zhang, H., Smith, J. L., and Cramer, W. A. (2003) *Science* **302**, 1009–1014
5. Stroebel, D., Choquet, Y., Popot, J. L., and Picot, D. (2003) *Nature* **426**, 413–418
6. Baniulis, D., Yamashita, E., Whitelegge, J. P., Zatsman, A. I., Hendrich, M. P., Hasan, S. S., Ryan C. M., and Cramer, W. A. (2009) *J. Biol. Chem.* **284**, 9861–9869
7. Berry, E. A., Guergova-Kuras, M., Huang, L. S., and Crofts, A. R. (2000) *Annu. Rev. Biochem.* **69**, 1005–1075
8. Cramer, W. A., Yan, J., Zhang, H., Kurisu, G., and Smith, J. L. (2005) *Photosynth. Res.* **85**, 133–143
9. Darrouzet, E., Cooley, J. W., and Daldal, F. (2004) *Photosynth. Res.* **79**, 25–44

10. Crofts, A. R. (2004) *Photosynth. Res.* **80**, 223–243
11. Lavergne, J. (1983) *Biochim. Biophys. Acta* **725**, 25–33
12. Kuras, R., Saint-Marcoux, D., Wollman, F. A., and de Vitry, C. (2007) *Proc. Natl. Acad. Sci. U.S.A.* **104**, 9906–9910
13. Lezhneva, L., Kuras, R., Ephritikhine, G., and de Vitry, C. (2008) *J. Biol. Chem.* **283**, 24608–24616
14. Alric, J., Pierre, Y., Picot, D., Lavergne, J., and Rappaport, F. (2005) *Proc. Natl. Acad. Sci. U.S.A.* **102**, 15860–15865
15. Baymann, F., Giusti, F., Picot, D., and Nitschke, W. (2007) *Proc. Natl. Acad. Sci. U.S.A.* **104**, 519–524
16. Ducluzeau, A. L., Chenu, E., Capowicz, L., and Baymann, F. (2008) *Biochim. Biophys. Acta* **1777**, 1140–1146
17. Yamashita, E., Zhang, H., and Cramer, W. A. (2007) *J. Mol. Biol.* **370**, 39–52
18. Musser, S. M., Stowell, M. H., Lee, H. K., Rumbley, J. N., and Chan, S. I. (1997) *Biochemistry* **36**, 894–902
19. Zhang, H., Primak, A., Cape, J., Bowman, M. K., Kramer, D. M., and Cramer, W. A. (2004) *Biochemistry* **43**, 16329–16336
20. Joliot, P., and Joliot, A. (1988) *Biochim. Biophys. Acta* **933**, 319–333
21. Choquet, Y., Zito, F., Wostrickoff, K., and Wollman, F. A. (2003) *Plant Cell* **15**, 1443–1454
22. Kuras, R., and Wollman, F. A. (1994) *EMBO J.* **13**, 1019–1027
23. Harris, E. H. (1989) *The Chlamydomonas Source Book: A Comprehensive Guide to Biology and Laboratory Use*, Academic Press, San Diego
24. Goldschmidt-Clermont, M. (1991) *Nucleic Acids Res.* **19**, 4083–4089
25. Boynton, J. E., Gillham, N. W., Harris, E. H., Hosler, J. P., Johnson, A. M., Jones, A. R., Randolph-Anderson, B. L., Robertson, D., Klein, T. M., and Shark, K. B. (1988) *Science* **240**, 1534–1538
26. de Lacroix de Lavalette, A., Barbagallo, R. P., and Zito, F. (2008) *C. R. Biol.* **331**, 510–517
27. Pierre, Y., Breyton, C., Kramer, D., and Popot, J. L. (1995) *J. Biol. Chem.* **49**, 29342–29349
28. Huang, D., Everly, R. M., Cheng, R. H., Heymann, J. B., Schägger, H., Sled, V., Ohnishi, T., Baker, T. S., and Cramer, W. A. (1994) *Biochemistry* **33**, 4401–4409
29. Bennoun, P., and Delepelaire, P. (1982) in *Methods in Chloroplast Molecular Biology* (Edelman, M., Chua, N. H., and Hallick, R. B., eds) pp. 25–38, Elsevier Biomedical Press
30. Zito, F., Kuras, R., Choquet, Y., Kössel, H., and Wollman, F. A. (1997) *Plant Mol. Biol.* **33**, 79–86
31. Lemaire, C., Girard-Bascou, J., and Wollman, F. A. (1987) in *Progress in Photosynthesis Research* (Biggins, J., ed) Vol. IV, pp. 655–658, Martinus Nijhoff Publishers
32. Joliot, P., Beal, D., and Frilley, B. (1980) *J. Chim. Phys.* **77**, 209–216
33. Cornforth, J. W., and James, A. T. (1956) *Biochem. J.* **63**, 124–130
34. Kuras, R., de Vitry, C., Choquet, Y., Girard-Bascou, J., Culler, D., Büschlen, S., Merchant, S., and Wollman, F. A. (1997) *J. Biol. Chem.* **272**, 32427–32435
35. Joliot, P., and Delosme, R. (1974) *Biochim. Biophys. Acta* **357**, 267–284
36. Junge, W., and Witt, H. T. (1968) *Z. Naturforsch. B.* **23**, 244–254
37. Selak, M. A., and Whitmarsh, J. (1984) *Photochem. Photobiol.* **39**, 485–489
38. Joliot, P., and Joliot, A. (2002) *Proc. Natl. Acad. Sci. U.S.A.* **99**, 10209–10214
39. Sacksteder, C. A., and Kramer, D. M. (2000) *Photosynth. Res.* **66**, 145–158
40. de Vitry, C., Desbois, A., Redeker, V., Zito, F., and Wollman, F. A. (2004) *Biochemistry* **43**, 3956–3968
41. Liu, Y., Moënné-Loccoz, P., Hildebrand, D. P., Wilks, A., Loehr, T. M., Mauk, A. G., and Ortiz de Montellano, P. R. (1999) *Biochemistry* **38**, 3733–3743
42. Hildebrand, D. P., Burk, D. L., Maurus, R., Ferrer, J. C., Brayer, G. D., and Mauk, A. G. (1995) *Biochemistry* **34**, 1997–2005
43. Andrew, C. R., Kemper, L. J., Busche, T. L., Tiwari, A. M., Kecskes, M. C., Stafford, J. M., Croft, L. C., Lu, S., Moënné-Loccoz, P., Huston, W., Moir, J. W., and Eady, R. R. (2005) *Biochemistry* **44**, 8664–8672
44. Streckas, T. C., and Spiro, T. G. (1974) *Biochim. Biophys. Acta* **351**, 237–245
45. Rich, P. R., Madgwick, S. A., and Moss, D. A. (1991) *Biochim. Biophys. Acta* **1058**, 312–328
46. Zhang, L., Yu, L., and Yu, C. A. (1998) *J. Biol. Chem.* **273**, 33972–33976
47. Muller, F., Crofts, A. R., and Kramer, D. M. (2002) *Biochemistry* **41**, 7866–7874
48. Muller, F. L., Roberts, A. G., Bowman, M. K., and Kramer, D. M. (2003) *Biochemistry* **42**, 6493–6499
49. Springer, B. A., Egeberg, K. D., Sligar, S. G., Rohlf, R. J., Mathews, A. J., and Olson, J. S. (1989) *J. Biol. Chem.* **264**, 3057–3060
50. Wilson, E. K., Bellelli, A., Liberti, S., Arese, M., Grasso, S., Cutruzzola, F., Brunori, M., and Brzezinski, P. (1999) *Biochemistry* **38**, 7556–7564
51. Perutz, M. F., Wilkinson, A. J., Paoli, M., and Dodson, G. G. (1998) *Annu. Rev. Biophys. Biomol. Struct.* **27**, 1–34
52. Adachi, S., Nagano, S., Ishimori, K., Watanabe, Y., Morishima, I., Egawa, T., Kitagawa, T., and Makino, R. (1993) *Biochemistry* **32**, 241–252
53. Das, T. K., Wilson, E. K., Cutruzzola, F., Brunori, M., and Rousseau, D. L. (2001) *Biochemistry* **40**, 10774–10781
54. Allen, J. F. (2004) *Trends Plant Sci.* **9**, 130–137